University of Hertfordshire UH

Link to the final published version available at the publisher:

https://doi.org/10.1093/mnras/sty220

Dense gas and star formation in individual Giant Molecular Clouds in M31

S. Viaene,[1,2]★ J. Forbrich[1,3] and J. Fritz[4]

[1]*Centre for Astrophysics Research, University of Hertfordshire, College Lane, Hatfield AL10 9AB, UK*
[2]*Sterrenkundig Observatorium, Universiteit Gent, Krijgslaan 281, B-9000 Gent, Belgium*
[3]*Harvard–Smithsonian Center for Astrophysics, 60 Garden St, Cambridge, MA 02138, USA*
[4]*Instituto de Radioastronomía y Astrofísica (IRyA-UNAM), Antigua Carretera a Pátzcuaro, 8701, Morelia, Michoacán, Mexico*

ABSTRACT

Studies both of entire galaxies and of local Galactic star formation indicate a dependency of a molecular cloud's star formation rate (SFR) on its dense gas mass. In external galaxies, such measurements are derived from HCN(1–0) observations, usually encompassing many Giant Molecular Clouds (GMCs) at once. The Andromeda galaxy (M31) is a unique laboratory to study the relation of the SFR and HCN emission down to GMC scales at solar-like metallicities. In this work, we correlate our composite SFR determinations with archival HCN, HCO^+, and CO observations, resulting in a sample of nine reasonably representative GMCs. We find that, at the scale of individual clouds, it is important to take into account both obscured and unobscured star formation to determine the SFR. When correlated against the dense-gas mass from HCN, we find that the SFR is low, in spite of these refinements. We nevertheless retrieve an SFR–dense-gas mass correlation, confirming that these SFR tracers are still meaningful on GMC scales. The correlation improves markedly when we consider the HCN/CO ratio instead of HCN by itself. This nominally indicates a dependency of the SFR on the dense-gas *fraction*, in contradiction to local studies. However, we hypothesize that this partly reflects the limited dynamic range in dense-gas mass, and partly that the ratio of single-pointing HCN and CO measurements may be less prone to systematics like sidelobes. In this case, the HCN/CO ratio would importantly be a better empirical measure of the dense-gas content itself.

Key words: ISM: clouds – galaxies: individual: M31 – galaxies: star formation.

1 INTRODUCTION

In recent years, a growing interest has developed in connecting Galactic and extragalactic studies of star formation, enabled by access to similar physical scales. The main synergy lies in connecting the level of detail of local studies with a wider range of physical conditions in observations of star formation in nearby galaxies. The main observational goal in both cases is to tie the occurrence of star formation to properties of the interstellar medium. The best-known extragalactic example is the empirical Kennicutt–Schmidt (KS) relation between the surface density of star formation and the surface density of the *total* (atomic and molecular) gas content of entire galaxies (Schmidt 1959; Kennicutt 1998).

At the same time, studies of star formation at local, Galactic scales, have reached an unprecedented level of detail, and it has become possible to both test extragalactic scaling relations and formulate new hypotheses. The main advantages over extragalactic studies are (1) more direct access to fundamental parameters such as masses and star formation rates (SFRs), for example by using extinction mapping and YSO counting (e.g. Lada, Lombardi & Alves 2010), and (2) the opportunity to validate methodologies of extragalactic measurements locally (e.g. Heiderman et al. 2010; Chomiuk & Povich 2011).

Based on a detailed sample of local clouds (d<500 pc), Lada et al. (2012) importantly argued that the KS relation does not explain star formation in the local clouds. Instead, they found that an empirical dense-gas scaling relation, where the SFR in a cloud depends linearly on its mass of dense gas, may be a more fundamental relation than the KS relation. Additionally, it both describes the local clouds and connects to similar reasoning for entire galaxies by Gao & Solomon (2004). In a follow-up study, Lada et al. (2013) concluded that a KS scaling relation only explains star formation within but crucially not between clouds. Cloud structure results in enhanced SFRs in regions with high column densities, but this does not necessarily imply a universal sharp (Heaviside) column density

threshold of star formation. They conclude that a dense-gas scaling relation provides a far better description of star formation in the local clouds than a global KS relation. In the case of the local clouds, this formalism results in a strong correlation of a cloud's SFR with the dense gas above $A_K > 0.8$ mag, as confirmed by Evans, Heiderman & Vutisalchavakul (2014) and Vutisalchavakul, Evans & Heyer (2016).

Other than column density mapping utilizing infrared extinction, which is only available for nearby clouds, gas of different volume densities can be observed with the help of molecular tracers. This is so far the best tool in external galaxies as demonstrated by the pioneering study of Gao & Solomon (2004) who found a linear relation for entire galaxies between the SFR, as estimated from the total infrared luminosity, and the dense gas mass, as determined from the luminosity of the HCN(1–0) transition. In a picture where the corresponding total gas mass is determined from CO observations, this scenario matches that described for the local clouds by Lada et al. (2012). Moving towards smaller scales, this picture based on infrared and HCN observations can be extended to regions of massive star formation in our Galaxy (Wu et al. 2005; Jackson et al. 2013, see also Stephens et al. 2016).

In the local clouds, the N_2H^+ molecule is a better tracer of dense and cold gas in comparison to HCN, as shown in particular in comparison with *Herschel* data (see e.g. Forbrich et al. 2014; Shirley 2015; Kauffmann et al. 2017; Pety et al. 2017). However, N_2H^+ is even more difficult to observe in external galaxies than HCN, and the focus in extragalactic studies so far thus has been on the latter molecule. Insights from local clouds provide promising support for such studies. In particular, the results of Lada et al. (2012) indicate that the dense-gas scaling relation based on HCN and CO from Gao & Solomon (2004) and Wu et al. (2005) and extinction mapping of local clouds could be put on the same scale with only minor modifications.

However, it has so far been difficult to test the correlation of HCN, CO, and the SFR in individual Giant Molecular Clouds (GMCs) of size <100 pc in nearby galaxies, even though extensive studies on kpc scales are becoming available (Usero et al. 2015; Bigiel et al. 2016). In one of the highest-resolution studies of the relation of dense gas and star formation in an external galaxy beyond the Magellanic Clouds so far, Chen et al. (2017) study a cloud complex in M51 in CO(1–0) and HCN(1–0) as well as in other transitions. At a common resolution of ~ 200 pc, they compare these measurements with infrared luminosities at 70 μm as an SFR tracer, and find that their results are compatible with those of Gao & Solomon (2004). In the Local Group, Braine et al. (2017) compiled a sample of GMCs in low-metallicity galaxies, effectively obtaining a resolution of ~ 100 pc. They find a positive trend between both HCN and HCO$^+$ emission and the SFR, but argue that abundance ratios can have a strong effect on the molecular line intensities in these low-metallicity environments.

One of the most important local laboratories for star formation is the Andromeda galaxy (M31). Due to its proximity, high spatial resolution of ~ 100 pc can already be reached with single-dish facilities like the IRAM 30-m telescope. With a considerable investment of observing time, Brouillet et al. (2005, hereafter B05) conducted the first and so far largest survey of HCN in M31 molecular clouds, with 16 pointings, providing us with a first sample of *individual GMCs throughout M31* with HCN detections, which Chen et al. (2017) have already shown to be broadly compatible with the relation found by Gao & Solomon (2004). However, previous extragalactic studies of HCN as a dense-gas tracer and its relation to the SFR have not only mostly focused on considerably

larger (kpc) scales but also on the total infrared luminosity as a simple SFR estimate. The latter becomes a less reliable tracer of the total star formation at the small scales in M31 (see Section 2).

Using the B05 measurements, we here present a first study of how improved SFR estimates, taking into account both obscured and unobscured star formation, relate to the dense gas content of individual GMCs in an external galaxy. We adopt the same distance to M31 as in B05, 780 kpc.

2 DATA AND SAMPLE

The starting point of our comparison is the sample of B05, who target 16 dark clouds in the disc of M31. These clouds have been observed using the IRAM 30-m telescope to detect the HCN and HCO$^+$ molecular lines. The clouds all belong to the disc of M31, with galactocentric radii between 2.4 and 15.5 kpc and are all covered in the CO(1–0) map[1] by Nieten et al. (2006). For clarity, the cloud coordinates can be found in Table A1, converted to RA and Dec. from the B05 positions.

Each pointing has a full width at half maximum (FWHM) of 27.5 arcsec (B05), which corresponds to a physical size of 104 pc along the major axis in the disc of Andromeda. To accurately measure the SFR in each pointing, we use the high-resolution (beamsize ~ 6 arcsec) SFR map created by Ford et al. (2013). They combined the *GALEX FUV* and *Spitzer*-MIPS 24 μm maps for Andromeda, and use the *Spitzer*-IRAC 3.6 μm map to correct both maps for the contribution of evolved stars. This is an important step for the SFR calculation in M31, as the contribution of evolved stars to both the *FUV* flux and dust heating is significant (see also Viaene et al. 2017, and references therein). The corrected *FUV* and 24 μm maps are converted into SFR based on the formalism of Leroy et al. (2008). This composite tracer is sensitive to a range of star formation time-scales, as discussed in Kennicutt & Evans (2012). We refer the reader to Ford et al. (2013) for more details.

The SFR and CO intensity of the B05 clouds are plotted in Fig. 1. For comparison, we also extract and plot these properties for all M31 molecular clouds found by Kirk et al. (2015), based on cold dust emission. In this plot, there are two things to note. First is that the small sample of B05 covers a wide range of CO and SFR values in Andromeda, with a slight bias towards high CO intensities. This is by design to increase the chances of HCN detections. Secondly, the correlation between CO and SFR is weak for both samples. For the molecular clouds in Andromeda, there is no strong link between the absolute content of molecular gas, and the rate of star formation. We note that these measurements are made for the same aperture size (i.e. one FWHM), so the correlation will not change when plotting surface density quantities.

3 DENSE GAS IN M31

The lack of correlation between CO intensity and SFR points towards a more subtle relationship between molecular gas and star formation. While the critical density for CO(1–0) lies around 10^3 cm^{-3}, this is much higher ($10^{5.7}$ cm^{-3}) for HCN(1–0) (Shirley 2015), making the transition more sensitive to dense molecular gas.

The HCN(1–0) emission line is detected in nine of the 16 pointings from B05. Before we go into the analysis of the dense gas

---

[1] While B05 use a preliminary version of this map, we use the published version. Excellent agreement was found between the quoted CO fluxes of B05 and our own measurements.
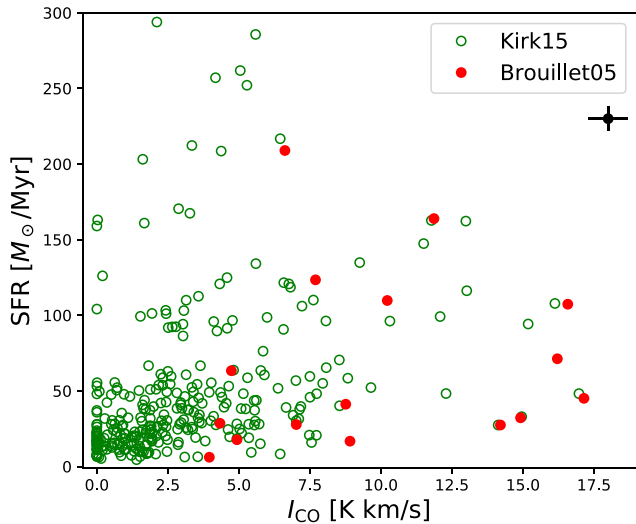
Figure 1. SFR as a function of integrated CO intensity for molecular clouds in Andromeda. The green points correspond to the catalogue of Kirk et al. (2015), and the red data points are the regions targeted by B05. The average uncertainties are shown in black in the top right corner.
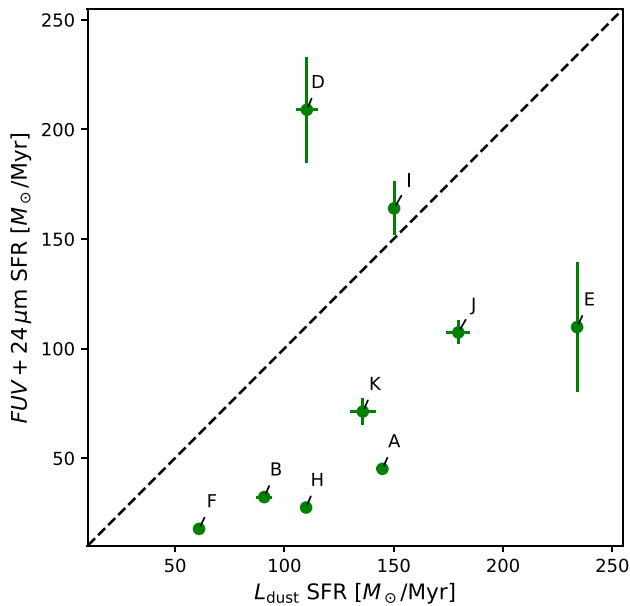
Figure 2. Comparison of the SFR for the HCN-detected regions. The SFR on the abscissa was derived as in Gao & Solomon (2004). This linearly scales with the total dust luminosity, computed from integrating the full infrared SED (Viaene et al. 2014). The SFR on the ordinate was derived from a combination of *FUV* and 24 μm emission, correcting for the contribution of evolved stars (Ford et al. 2013). The black dashed line indicates a 1:1 correspondence.

properties of these clouds, we compare our new SFR estimate (from the Ford et al. 2013 map) with what one would obtain following the classic linear conversion between SFR and the total dust luminosity (see equation 9 in Gao & Solomon 2004). While this is the preferred SFR tracer in previous HCN–SFR studies (see e.g. Usero et al. 2015, for an overview), we do not find a clear correspondence on physical scales of 100 pc (see Fig. 2). Some of the pointings, notably clouds D and I, exhibit clear signs of unobscured

star formation (see Fig. A1). This is not picked up in L_{dust}, but is incorporated in the $FUV + 24 \mu\text{m}$ tracer. On larger scales, one can expect the fraction of obscured SFR to dominate, especially in the dust-rich star-forming galaxies which were investigated so far.

In addition, L_{dust}-based SFRs generally yield higher rates of star formation. This is particularly true for M31, where the dust is in fact mainly heated (60–90 per cent for these regions) by evolved stars (Viaene et al. 2017), thus artificially increasing this SFR estimate. In the remainder of this work, we therefore rely on the composite SFR tracer, which includes unobscured star formation, and where the contribution of the evolved stars has been removed.

With our more comprehensive SFR estimate we confirm a general trend between HCN line emission and the SFR (see the top left panel in Fig. 3), with a Spearman correlation coefficient R of 0.62. For completeness, we also include the HCO^+ line intensities in Fig. 3 (top right panel). There is still a positive correlation, but the scatter is larger ($R = 0.36$).

We find an even better correlation when plotting the SFR against the HCN/CO ratio (Fig. 3, lower left panel). We find a correlation coefficient of $R = 0.63$, drastically improving to $R = 0.98$ when removing the marginal outlier point F (see below). Both values only leave a small chance that this correlation is a statistical coincidence. A linear fit to the data, taking into account their uncertainties, yields

$$\text{SFR} = (88 \pm 11)X_N - (50 \pm 16), \qquad (1)$$

which yields SFR in $M_\odot \, \text{Myr}^{-1}$ from $X_N = 100 I_{\text{HCN}}/I_{\text{CO}}$.

The trend between SFR and the HCO^+/CO line ratio also improves when compared to the SFR versus HCO^+ relation, but the scatter is slightly larger ($R = 0.75$). Braine et al. (2017) recently noted that these line ratios are indeed positively correlated with the 24 μm flux, a proxy for obscured star formation. Their sample was a set of GMCs in low-metallicity Local Group galaxies at a comparable physical resolution ~100 pc. Fig. 3 presents, to our knowledge, the first comparison for extragalactic GMCs at ~100 pc scales in a normal-metallicity environment. In the remainder of the paper, we explore the strongest relationship (SFR versus X_N) in more depth.

First, we perform a rigorous error analysis. The lower left panel in Fig. 3 shows a notable outlier: cloud F, the pointing with the lowest SFR and only a marginal, low-S/N HCN detection. In the uncertainty on each SFR measurement, we include the basic uncertainty in the SFR map (taken from Ford et al. 2013), plus a positional uncertainty – mainly since we do not know the relative positional accuracy of the various maps used here. We perform a bootstrapping analysis, creating 10 000 new pointings drawn from a normal probability distribution centred at the original pointing, with a conservatively[2] chosen spread of 6.9 arcsec (1/4 times the IRAM FWHM beam). This yields an average pointing uncertainty of 8 per cent in SFR, which is the dominant error.

Analogously, we find an average pointing uncertainty of 5 per cent from the CO map. We combine this with the HCN detection uncertainties quoted in B05 for the uncertainty on X_N. Note that the uncertainties quoted on the HCN emission are already conservative estimates based on the information provided in B05. The uncertainties on X_N are comparable with the scatter in the X_N–SFR relationship, which is reassuring. The only exception is indeed cloud F, which turns out to have a large uncertainty (51 per cent) on the HCN detection. B05 already noted that this cloud may be quiescent, and treat it as an outlier in their further analysis. Given the high uncertainty enshrouding the HCN detection in cloud F, we do

---

[2] Nieten et al. (2006) report a pointing uncertainty of <5 arcsec.
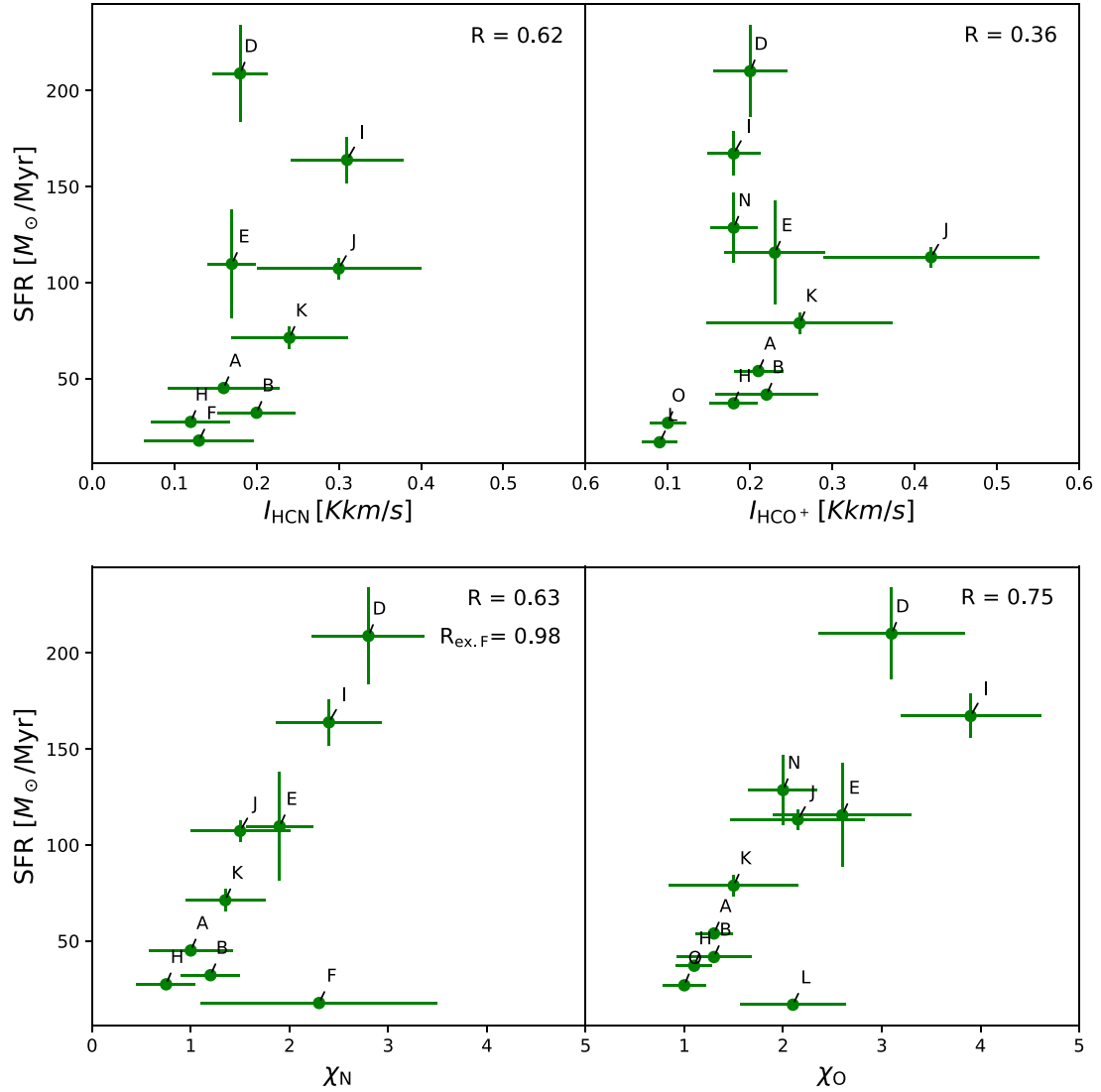
Figure 3. Star formation and dense gas in the clouds detected by B05. Top row: total SFR versus the HCN and HCO$^+$ integrated line intensities. Bottom row: total SFR as a function of the HCN/CO and HCO$^+$/CO line ratios, X_N and X_O, respectively (in percent). The Spearman rank coefficient R is shown in the top right of each panel. The errors are conservatively estimated to reflect an assumed relative positional uncertainty of 1/4 IRAM beam, plus the measurement uncertainty on the parameters themselves.

not speculate any further on the nature of this outlier. We note that the Spearman coefficient becomes $R = 0.98$ when removing point F, and the *p*-value becomes 3.3×10^{-5}, making the correlation much more significant.

Secondly, we test this correlation using an independent measure of the SFR. We chose to use a combination of Hα luminosity and total dust luminosity, following the prescription of Kennicutt & Evans (2012). The Hα map from Devereux et al. (1994) was used, combined with the map of total dust luminosity from Viaene et al. (2014). The X_N versus SFR correlation for this particular calibration is shown in the bottom panel of Fig. 4. The same trend arises (including outlier F), although shifted to slightly higher SFR. We suspect this is due to evolved stars contributing to the dust heating in M31 (see Viaene et al. 2017), which is not subtracted in the $L_{H\alpha} + L_{dust}$ calibration, but is corrected for in the $FUV + 24\,\mu m$ calibration. It is not the goal of this paper to compare SFR tracers, so we will continue to use the composite $FUV + 24\,\mu m$ tracer in the remainder of this work.

The HCN line intensities can be converted to a dense gas mass. We assume $\alpha_{HCN} = 10\,M_\odot\,(K\,km\,s^{-1}\,pc^2)^{-1}$ to remain consistent with Gao & Solomon (2004). This yields M_{HCN} of $1 - 3 \times 10^4\,M_\odot$. Fig. 5 shows their relation to the SFR, together with the SFR–dense gas mass relation found by Lada et al. (2012) for local Milky Way clouds. Their SFR is based on counting young stellar objects and they find a calibration offset of 2.7 with respect to the Gao & Solomon (2004) relation. We therefore also show the Lada et al. (2012) relation, divided by 2.7.

While a weak trend exists between the dense gas mass and the SFR, the data do not match either of the above two relations. This was already noted by Chen et al. (2015), who compared the B05 regions in the L_{IR}–L_{HCN} parameter space to sub-kpc regions in M51 and global galaxy measurements. They find that the M31 regions lie below the main trend, which is also reflected in Fig. 5. The average L_{IR}/L_{HCN} ratio is $433 \pm 175\,L_\odot(K\,km\,s^{-1}\,pc^2)^{-1}$ for the M31 regions. This lies well below the Gao & Solomon (2004) ratio $[900\,L_\odot(K\,km\,s^{-1}\,pc^2)^{-1}]$, but in between the values for central
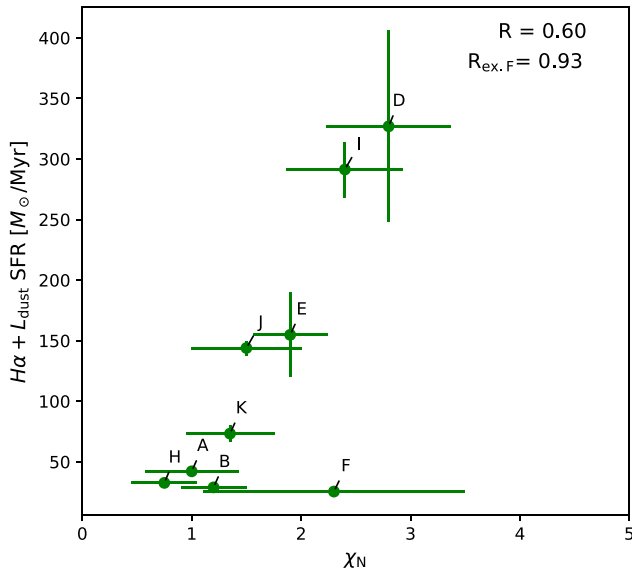
Figure 4. SFR as a function of the HCN/CO line ratio, X_N. This SFR estimated is based on Hα + L_{dust} emission. The errors are conservatively estimated to reflect an assumed relative positional uncertainty of 1/4 IRAM beam, plus the uncertainty on the SFR and X_N itself.
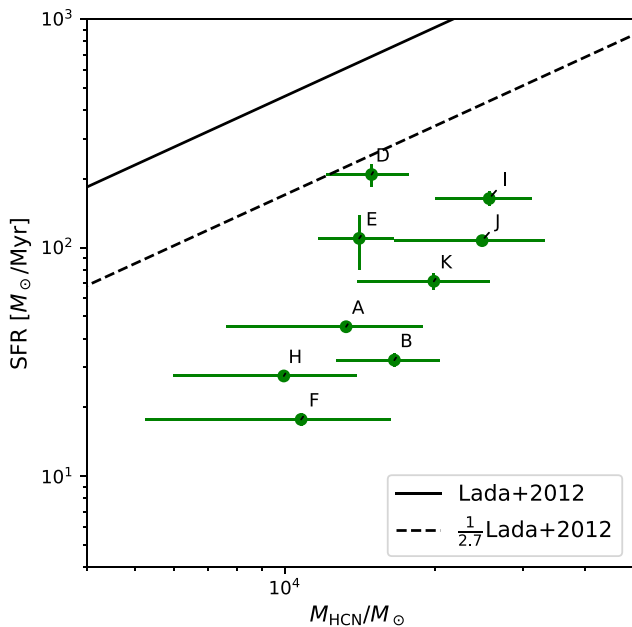
Figure 5. SFR as a function of dense gas mass as traced by HCN(1–0) (M_{HCN}). The solid black line corresponds to the Lada et al. (2012) relation for local Milky Way clouds. The dashed line is the same relation, but rescaled to correspond to the Gao & Solomon (2004) data.

regions in M51 [$388 \pm 47 \, \text{L}_\odot (\text{K km s}^{-1} \, \text{pc}^2)^{-1}$] and regions in the outer disc of M51 [$691 \pm 156 \, \text{L}_\odot \, (\text{K km s}^{-1} \, \text{pc}^2)^{-1}$].

In addition to the intrinsic offset to the Gao & Solomon (2004) relation, Fig. 2 also reveals an important offset between L_{IR}-based SFR and our composite tracer. The combination of these two effects leads to rather high nominal dense-gas depletion times for the M31 clouds, which lie between 70 and 600 Myr, although the uncertainties in the latter are substantial, driven by the uncertainties in the HCN masses.

4 DISCUSSION

4.1 GMC properties

Before moving on to interpret their behaviour, it is important to verify the nature of the structures under investigation, and reflect on our methods to estimate their properties.

First, we verify the class of the probed regions. B05 classify them as GMCs, based on the CO map, which has limited resolution (23 arcsec beam). We reassess their classification by inspecting composite *gri* SDSS images[3] of the target areas (see Fig. A1). The optical colour maps provide a better resolution (1–2 arcsec seeing) than the CO map, and the denser ISM can be traced efficiently through reddening by dust. The HCN-detected clouds can all be associated with continuous structures of dust extinction. These structures are several 100 pc in size, with multiple star-forming regions, suggesting they are giant molecular associations (GMAs). The HCN pointings pick up entities ($\sim$100 pc in diameter) within these structures. This confirms the classification of B05 in that we are most likely tracing individual GMCs.

Secondly, it is difficult to assess whether we are observing the same physical structure in CO, HCN and in the SFR map. The latter has a resolution of 6 arcsec, so we summed pixels within a circular aperture of diameter 27.5 arcsec. As discussed above, we then allow for the possibility of offsets between the SFR, CO, and HCN maps when cross-matching the data. This ensures that any significant source structure that falls just outside of the nominal beam at least gets included in the error budget.

Thirdly, the inclined view of the M31 disc ($i \sim 77°$) can cause line-of-sight effects. Two of the pointings (A and E) have two distinct velocity components, suggesting there are at least two different structures in the beam along the line-of-sight. In both cases, we used the ones with the highest HCN intensity (which corresponds to the highest CO intensity as well). However, for the SFR estimate, we have no velocity information and are in essence summing up the combined signal along the line-of-sight. However, even without pointings A and E, the correlation would persist. Nevertheless, it is possible that there are more unknown offsets between the origin of HCN, CO and SFR within the 100 pc beam, or along the line-of-sight. Future interferometric studies could resolve such offsets.

4.2 Star formation rates

We find unusually low SFRs for the M31 GMCs. They are a factor of 2–3 lower than those from L_{dust}, which in turn are a factor of 2.7 lower than SFRs from YSO counting (Chomiuk & Povich 2011; Lada et al. 2012), resulting in SFRs that are almost an order of magnitude lower than calibrations suggested by YSO counting. This in turn leads to unusually long and unrealistic depletion times of up to 600 Myr. The difference could point to stochastic sampling of star formation in these regions. If the SFR calibration assumes a fully sampled IMF and instead individual regions may have less overall emission from massive stars, then the resulting SFRs will be biased towards lower numbers.

Alternatively, individual clouds could have star formation time-scales different from those usually assumed for star-formation recipes calibrated for extragalactic studies. However, Kennicutt & Evans (2012) report a mean age range of 3, 5, 5, and 10 Myr for Hα, 24 µm, TIR, and FUV, respectively. These are still relatively short

---

[3] http://www.sciserver.org

time-scales, which are realistic even for individual clouds where stars are formed on a short time-scale. SFR scaling relations are expected to break down at small spatial scales (see e.g. Kennicutt & Evans 2012; Kruijssen & Longmore 2014). The SFR map of Ford et al. (2013) has a resolution of 6 arcsec, but we sum all pixels within a circle of 27.5 arcsec diameter. The SFR calibration is linear, which means our effective resolution is still 100 pc.

Scaling relations involving SFR were found to be still valid at 140 pc scales in M31 (Viaene et al. 2014), albeit with some scatter. Also, despite the above concerns, we still observe a tight correlation between SFR and X_N. This indicates that, if not the absolute calibration, at least the relative differences in SFR are genuine, even for GMC-sized structures. A detailed study of the role of physical scales is beyond the scope of this paper since it will have to be addressed with more comprehensive dense-gas and SFR data.

4.3 SFR and the HCN/CO ratio

Our results suggest a strong connection between the SFR and the HCN/CO line ratio. This ratio is often interpreted as a dense gas fraction since it was thus proposed by Gao & Solomon (2004). These authors find constant HCN/CO ratios for star-forming galaxies, but a higher ratio for starburst galaxies. In the local Milky Way clouds studied by Lada et al. (2012), a clear linear link between the absolute dense gas mass (derived from dust extinction) and the SFR excludes a tight correlation between the SFR and the HCN/CO ratio. These two studies both cover a dynamic range of two orders of magnitude in dense gas mass. Due to sensitivity limitations, our M31 sample is limited to a dynamic range in the dense gas mass of a factor of about only 2.4 and by a factor of about 7.5 in the total gas mass. Despite this limitation, which allows only for a tentative search for trends, clear correlations still emerge, and using the HCN/CO ratio leverages the larger dynamic range of the CO measurements.

The reliability of HCN as a tracer of dense gas is a matter of ongoing debate (see e.g. Costagliola et al. 2011; Barnes et al. 2017; Kauffmann et al. 2017; Pety et al. 2017; Schap et al. 2017, and references therein). Collisional excitation produces HCN(1–0) emission above a critical density, and our understanding of collisional excitation continues to improve (Hernández Vera et al. 2017), but depending on the environmental conditions, observable emission may occur at densities significantly below the critical density (e.g. Goldsmith & Kauffmann 2017). Infrared pumping of HCN is also possible (see e.g. Imanishi, Nakanishi & Izumi 2017), but only when a very bright MIR source (e.g. an AGN) is present. Gao & Solomon (2004) did not find evidence for IR pumping in their sample, and even in extreme cases, the contribution to the line emission remains below 20 per cent (Vollmer et al. 2017). Additionally, M31 has a well-known metallicity gradient (Mattsson et al. 2014), which can change the amount of nitrogen in the gas phase and thus change HCN abundances. Nonetheless, one can argue that, globally, the physical conditions of the regions in this work are comparable since all of them are part of the disc of M31.

The apparent link between SFR and the HCN/CO ratio does not necessarily imply a physical contradiction with the locally observed correlation between the SFR and the dense-gas mass. Our hypothesis would instead be that when considering single-pointing measurements on cloud scales, the ratio of HCN and CO could be the empirically cleanest measure of the dense gas content. Determining the dense-gas mass from a single pointing may be impacted by systematic effects from additional parameters, like beam sidelobes, hence the poorer correlation in Fig. 5.

Deriving M_{HCN} requires the explicit assumption of a size scale (the FWHM main beam) where all emission is thought to be contained. Since there is only one pointing per cloud, we do not know a priori how well-justified this assumption is. If, for example, the molecular peak or any other significant emission is outside of the FWHM beam, the ratio of HCN/CO, both affected in similar ways from emission caught in the outer sensitivity pattern, may be a better empirical measure of the dense-gas content of the inner cloud than just HCN, assumed to originate from within the FWHM beam and thus in tendency under-estimated if the peak is outside of the main beam.

It is clear that the observed correlation raises several intriguing questions, and can reveal unknown aspects of star formation on cloud scales. However, the limited sample size largely prevents us from drawing firm conclusions. A larger sample of molecular clouds and spatially resolved maps is needed to confirm the exact nature of the correlation.

5 SUMMARY AND CONCLUSIONS

In our comparison of the dense gas content and SFRs of individual GMCs at the scale of 100 pc in M31, we find the following.

(i) To inspect the target regions further, at the highest available resolution, we study them qualitatively in optical dust extinction. We conclude that the HCN pointings contain small fractions of GMAs, and most likely individual GMCs.

(ii) At these scales, a composite (obscured + unobscured) SFR tracer is preferred over the total infrared luminosity as several clouds show clear evidence of unobscured star formation. Also, this tracer importantly corrects for significant dust heating by evolved stellar populations.

(iii) This sample of GMCs in M31 is covering a representative dynamic range in both SFR and CO luminosity when compared to analogous measurements for a comprehensive cloud catalogue.

(iv) For the nine GMCs with an HCN detection, the SFR correlates with the HCN and HCO$^+$ luminosities and thus dense gas mass. This correlation is broadly consistent with previous extragalactic and Galactic results.

(v) The correlation with SFR improves considerably when instead of the HCN luminosity we consider the ratio of the clouds' HCN and CO luminosities. A similar but weaker effect is seen when considering the HCO$^+$ emission.

(vi) This correlation suggests that the SFR estimates are useful, even on these small scales, but not necessarily in an absolute sense since the resulting nominal depletion times are too long when compared to individual local clouds.

In the picture originally proposed by Gao & Solomon (2004), where the total mass of a cloud is measured in CO and the dense-gas mass is measured in HCN, our finding thus would suggest a correlation of the SFR with a nominal dense gas *fraction* on cloud scales, in contradiction to local results. However, we hypothesize that the reason for this improved correlation is partly due to (a) the limited dynamic range in the dense gas mass, such that the HCN/CO ratio leverages the larger dynamic range in total gas mass from CO measurements, and (b) systematic uncertainties that are shared by both the HCN and CO measurements, such that they cancel out in the ratio. Importantly, the HCN/CO line ratio would then correspond to a measure of the dense gas mass for this specific case of individual single-dish measurements.

REFERENCES

Barnes A. T., Longmore S. N., Battersby C., Bally J., Kruijssen J. M. D., Henshaw J. D., Walker D. L., 2017, MNRAS, 469, 2263

Bigiel F. et al., 2016, ApJ, 822, L26

Braine J., Shimajiri Y., André P., Bontemps S., Gao Y., Chen H., Kramer C., 2017, A&A, 597, A44

Brouillet N., Muller S., Herpin F., Braine J., Jacq T., 2005, A&A, 429, 153 (B05)

Chen H., Gao Y., Braine J., Gu Q., 2015, ApJ, 810, 140

Chen H., Braine J., Gao Y., Koda J., Gu Q., 2017, ApJ, 836, 101

Chomiuk L., Povich M. S., 2011, AJ, 142, 197

Costagliola F. et al., 2011, A&A, 528, A30

Devereux N. A., Price R., Wells L. A., Duric N., 1994, AJ, 108, 1667

Evans II N. J., Heiderman A., Vutisalchavakul N., 2014, ApJ, 782, 114

Forbrich J., Öberg K., Lada C. J., Lombardi M., Hacar A., Alves J., Rathborne J. M., 2014, A&A, 568, A27

Ford G. P. et al., 2013, ApJ, 769, 55

Gao Y., Solomon P. M., 2004, ApJ, 606, 271

Goldsmith P. F., Kauffmann J., 2017, ApJ, 841, 25

Heiderman A., Evans II N. J., Allen L. E., Huard T., Heyer M., 2010, ApJ, 723, 1019

Hernández Vera M., Lique F., Dumouchel F., Hily-Blant P., Faure A., 2017, MNRAS, 468, 1084

Imanishi M., Nakanishi K., Izumi T., 2017, ApJ, 849, 29

Jackson J. M. et al., 2013, PASA, 30, e057

Kauffmann J., Goldsmith P. F., Melnick G., Tolls V., Guzman A., Menten K. M., 2017, A&A, 605, L5

Kennicutt Jr R. C., 1998, ARA&A, 36, 189

Kennicutt R. C., Evans N. J., 2012, ARA&A, 50, 531

Kirk J. M. et al., 2015, ApJ, 798, 58

Kruijssen J. M. D., Longmore S. N., 2014, MNRAS, 439, 3239

Lada C. J., Lombardi M., Alves J. F., 2010, ApJ, 724, 687

Lada C. J., Forbrich J., Lombardi M., Alves J. F., 2012, ApJ, 745, 190

Lada C. J., Lombardi M., Roman-Zuniga C., Forbrich J., Alves J. F., 2013, ApJ, 778, 133

Leroy A. K., Walter F., Brinks E., Bigiel F., de Blok W. J. G., Madore B., Thornley M. D., 2008, AJ, 136, 2782

Mattsson L. et al., 2014, MNRAS, 444, 797

Nieten C., Neininger N., Guélin M., Ungerechts H., Lucas R., Berkhuijsen E. M., Beck R., Wielebinski R., 2006, A&A, 453, 459

Pety J. et al., 2017, A&A, 599, A98

Schap W. J., Barnes P. J., Ordoñez A., Ginsburg A., Yonekura Y., Fukui Y., 2017, MNRAS, 465, 2559

Schmidt M., 1959, ApJ, 129, 243

Shirley Y. L., 2015, PASP, 127, 299

Stephens I. W., Jackson J. M., Whitaker J. S., Contreras Y., Guzmán A. E., Sanhueza P., Foster J. B., Rathborne J. M., 2016, ApJ, 824, 29

Usero A. et al., 2015, AJ, 150, 115

Viaene S. et al., 2014, A&A, 567, A71

Viaene S. et al., 2017, A&A, 599, A64

Vollmer B., Gratier P., Braine J., Bot C., 2017, A&A, 602, A51

Vutisalchavakul N., Evans II N. J., Heyer M., 2016, ApJ, 831, 73

Wu J., Evans II N. J., Gao Y., Solomon P. M., Shirley Y. L., Vanden Bout P. A., 2005, ApJ, 635, L173

## APPENDIX A: CLOUD SAMPLE

The coordinates for the clouds in the sample of B05 are listed in Table A1, as are their SFRs. Composite SDSS colour maps are shown in Fig. A1.

Table A1. Coordinates, SFRs, and relative uncertainties for the B05 pointings. SFR is based on the FUV+24 micron map of Ford et al. (2013).

Pointing	RA J2000	DEC. J2000	SFR ($M_\odot$ Myr^{-1})	σ_{SFR}^{rel}
A	00:41:05.02	+40:38:01.7	45.1	0.04
B	00:41:13.91	+41:08:37.9	32.2	0.09
C	00:41:04.99	+40:37:31.7	41.2	0.05
D	00:41:30.14	+41:04:53.7	209.0	0.20
E	00:41:00.45	+41:03:31.1	109.8	0.42
F	00:42:41.13	+41:07:19.9	17.7	0.09
G	00:44:26.88	+41:38:01.1	27.7	0.11
H	00:44:13.09	+41:35:12.6	27.4	0.03
I	00:43:56.69	+41:26:34.1	163.9	0.13
J	00:42:38.57	+41:31:51.7	107.3	0.08
K	00:42:31.99	+41:29:46.8	71.2	0.12
L	00:44:02.85	+41:42:40.2	06.1	0.05
M	00:43:29.35	+41:48:48.4	63.4	0.11
N	00:44:43.38	+41:27:51.1	123.4	0.21
O	00:43:06.53	+41:24:15.4	16.8	0.12
P	00:42:56.73	+41:14:32.8	28.6	0.07
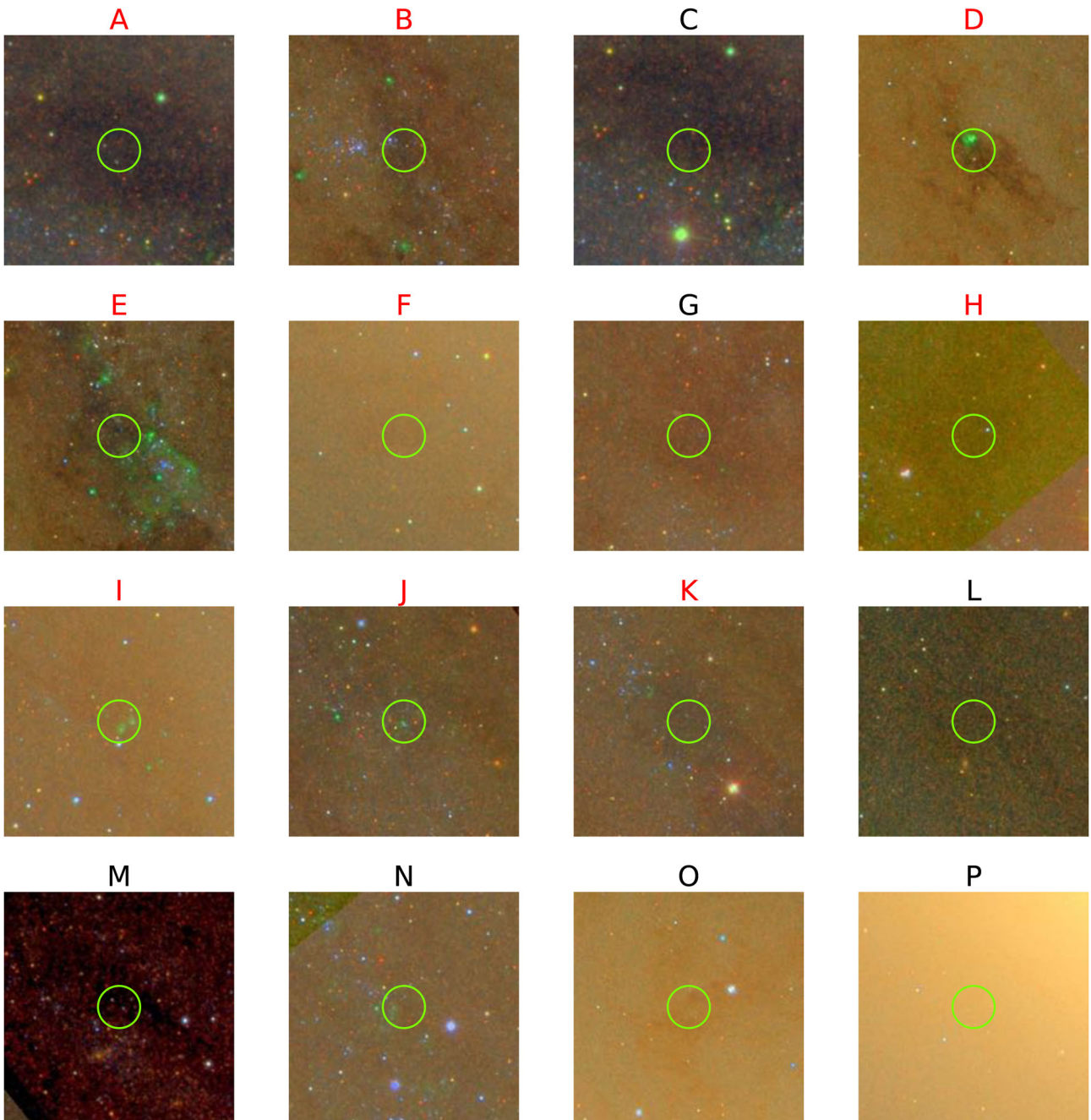
Figure A1. Composite SDSS *g* (blue), *r* (green), *i* (red) colour images for the regions targeted by B05. The green circle indicates the pointing and beam FWHM (27.5 arcsec). HCN-detected pointings are marked with a red label.

This paper has been typeset from a TEX/LATEX file prepared by the author.